Numerical investigation of draw bending and deep drawing taking into account cross hardening

Clemens Barthel, Till Clausmeyer, Bob, Svendsen
University of Technology,
Dortmund, Germany

Summary:

Sheet metal forming involves large strains and severe strain-path changes. Large plastic strains lead in many metals to the development of persistent dislocation structures resulting in strong flow anisotropy. This induced anisotropic behavior manifests itself in the case of a strain path change in very different stress-strain responses depending on the type of the strain-path change. While many metals exhibit a drop of the yield stress (Bauschinger effect) after a load reversal, some metals show an increase of the yield stress after an orthogonal strain-path change (so-called cross hardening). To model the Bauschinger effect, kinematic hardening has been successfully used for years. However, the usage of the kinematic hardening leads automatically to a drop of the yield stress after an orthogonal strain-path change contradicting tests exhibiting the cross hardening effect. In this work we present a phenomenological material model whose structure is motivated by polycrystalline modeling that takes into account the evolution of polarized dislocation structures on the grain level - the main cause of the induced flow anisotropy on the macroscopic level. The model considers besides the movement of the yield surface and its proportional expansion, as it is the case in conventional plasticity, also the changes of the yield surface shape (distortional hardening) and accounts for the pressure dependence of the flow stress. The model is applied to the simulation of a strip which is drawn over a roller at an angle of 90° with a specified tension. Later it is released which leads to a high amount of spring-back. The final shape of the strip is compared with the experiments. The agreement between the simulated shape and the real shape is very good. The second process which was investigated is the deep drawing of an axially symmetric cup. The model that takes into account the cross hardening shows in the regions where the blank is compressed and bent higher stresses as in the case of combined hardening. The material for the experiments was LH800 steel that has a ferritic micro structure. Experiments with load reversal and orthogonal loading path change have been carried out as basis for the identification of the different hardening parameters in the simulation.

Keywords:

induced flow anisotropy, distortional hardening, cross hardening, strain-path changes, pressure dependent plasticity, sheet forming, draw-bending, deep drawing

1 Material model

1.1 Introduction

Metal forming processes like draw bending or deep drawing lead to a large plastic deformation of the material. During deep drawing of a cup the material is drawn over a radius experiencing bending and back bending. Since the diameter of the cup is smaller compared to the initial blank, compression occurs in the circumferential direction. Thus severe strain path changes are involved in the process. Large plastic strains lead to flow anisotropy in many metals. This induced anisotropic behavior manifests itself in the case of a strain path change by different stress-strain responses depending on the type of the strain path change. While many metals exhibit a drop of the yield stress (Bauschinger effect) after a load reversal, some metals show an increase of the yield stress after an orthogonal strain path change (so-called cross hardening effect). The reason for this induced flow anisotropy is the development of persistent dislocation structures during large deformations. These consist of walls of high dislocation density separating low dislocation density areas. The one side of each wall contains excess dislocations of the same sign, and the other side such dislocations of the opposite sign. After a load reversal, plastic deformation takes place due to the slip on the same slip systems but in opposite direction. Excess dislocations, since they repel each other, facilitate this slip, resulting in the Bauschinger effect. After an orthogonal strain path change, new slip systems are activated and the existing dislocation walls act as obstacles, resulting in the cross hardening effect. A material model which takes these different hardenings into account will be shown in what follows.

1.2 Material testing

The material dealt with in this paper is the steel LH800 which is provided by Salzgitter Flachstahl AG. LH stands for the German word “lufthaertend” which means air hardening. The micro structure of LH800 is ferritic. During heating ferrite transforms into austenite. The transformation temperature is about 900° C. During cooling the austenite transforms directly into martensite or into bainite and martensite. When the LH800 is cooled down on the air it transforms almost completely into martensite. Since martensite is harder than ferrite the strength of the LH800 after the heat treatment is much higher but formability is reduced. The experiments and simulations shown in this paper deal with the not heat treated material. The material behavior was investigated for monotonic loading, reversed loading and orthogonal loading [1] [2]. Fig. 1 shows the result of a uniaxial tension test according to DIN EN 10002. Stress and strain are given as engineering values. The initial yield stress for the not heat treated material is about 370 MPa and the strength is about 470 MPa. In Fig. 2 the result of a tension-compression experiment can be seen. In order to prevent buckling in the compression stage the specimen had to be small. The area between the clamps is tailored and has a length of 10 mm. The drop of the yield stress after the load reversal clearly can be seen. Whereas the yield stress at the end of the tension stage is over 400 MPa in the compesson stage the yielding starts at -320 MPa. Thus the LH800 shows the Bauschinger-effect.

If not very pronounced the cross hardening effect can be seen when the material experiences an orthogonal loading path change. This becomes clear from (Fig. 3) where a sample is loaded in tension followed by shearing. Compared to a sample which is sheared from the beginning an increase of the yield stress after the orthogonal strain path change can be seen. Additionally reversed shear tests were performed where the kinematic hardening also can be seen. Finally Fig. 4 shows a bending test where a specimen is bent to an angle of 180 degrees followed by back-bending. This can be repeated for several cycles. With this test high plastic strains can be achieved. Unlike the previous tests the stress distribution is not homogeneous in this experiment. By turning the specimen about 90 degrees after the first cycles an orthogonal loading can be released.The experimental results show that LH800 exhibits a drop of the yield stress after a load reversal and an increase of the yield stress after an orthogonal strain path change. The Bauschinger effect and the so called cross hardening are present. The experiments are the basis for the parameter identification which, however, is not subject of this paper.

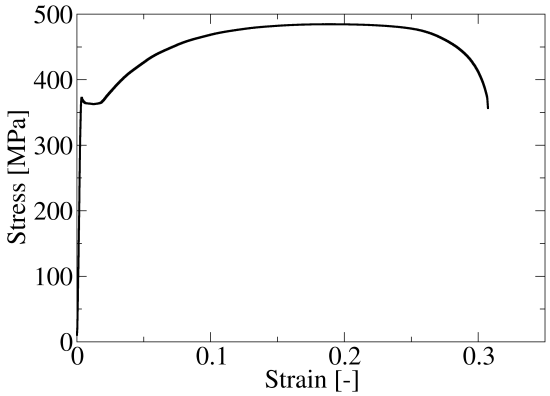

Figure 1: Uniaxial tension experiment (DIN EN 10002) (Experiments IW Hannover)

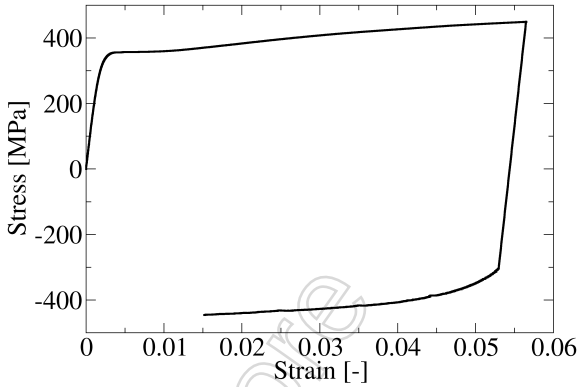

Figure 2: Tension-Compression experiment (Experiments IW Hannover)

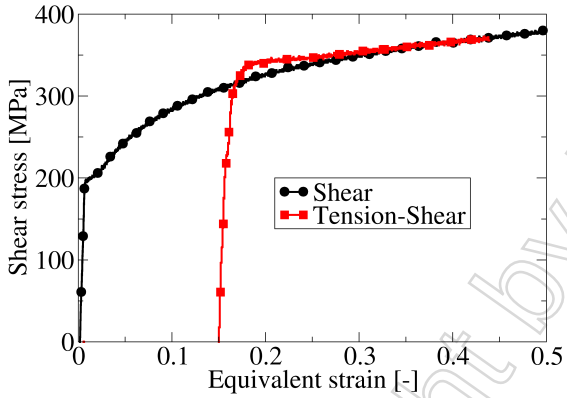

Figure 3: Tension-Shearing experiment (Experiments M2I Twente)

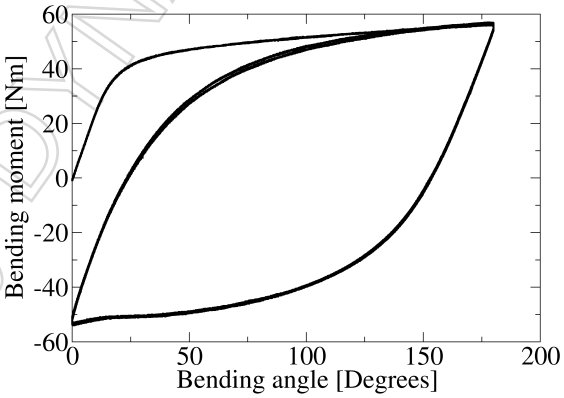

Figure 4: Bending experiment (Experiments University of Eindhoven)

1.3 Model description

The model which is presented here is capable of taking into account all the different hardening effects which seem to be present in LH800 [3].

The current model is based on the standard elasto-plastic framework with the yield function

$$\phi = \sigma_e + \alpha \mathrm{tr}(\mathbf{T}) - \sigma_{Y0} - R \tag{1}$$

where R is the yield stress, whose evolution is determined by Voce isotropic hardening, α is a material parameter, governing the plastic flow pressure sensitivity, and

$$\sigma_e = \sqrt{\mathbf{S} \cdot \mathscr{A} \mathbf{S}} \tag{2}$$

represents the equivalent stress measure.

Here

$$\mathbf{S} = \mathrm{dev}(\mathbf{T}) - \mathbf{X} \tag{3}$$

is the difference between the deviatoric part of the Cauchy stress **T** and the back stress **X**.

The plastic strain rate is given by the associative flow rule

$$\mathbf{D}_p = \dot{\lambda}\frac{\partial \phi}{\partial \mathbf{S}} = |\mathbf{D}_p|\,\mathbf{N} \tag{4}$$

where **N** is the direction of the plastic strain rate.

The evolution of the kinematic hardening is given by the Armstrong-Frederick relation

$$\dot{\mathbf{X}} = C_X(X_{Sat}\mathbf{D}_p - \mathbf{X})\dot{\lambda} \tag{5}$$

The $\mathscr{A}$ in eq. 2 is composed of two parts

$$\mathscr{A} = \mathscr{A}_T + \mathscr{H} \tag{6}$$

where $\mathscr{A}_T$ is the orthotropic Hill tensor. The fourth-order tensor $\mathscr{H}$, representing distorsional hardening, is described by the following evolution equation

$$\dot{\mathscr{H}} = c_D[h_D^{sat}\mathbf{N}\otimes\mathbf{N} - \mathscr{H}_D]\dot{\lambda} + c_L[h_L^{sat}(\mathscr{I}_{\text{dev}} - \mathbf{N}\otimes\mathbf{N}) - \mathscr{H}_{\mathscr{L}}]\dot{\lambda} \tag{7}$$

Here $\mathscr{I}_{\text{dev}}$ is the deviatoric part of the fourth-order identity tensor and **N** the direction of the plastic strain rate. Analogous to a vector which can be projected in the direction of another vector the $\mathscr{H}$-Tensor can be projected in the direction of $\mathbf{N}\otimes\mathbf{N}$. The first summand in the evolution equation for $\mathscr{H}$ (eq.7) is parallel to $\mathbf{N}\otimes\mathbf{N}$ and the second summand is perpendicular to $\mathbf{N}\otimes\mathbf{N}$ which means that the scalar product between the second summand in eq. 7 and $\mathbf{N}\otimes\mathbf{N}$ is zero.

The evolution equation for $\mathscr{H}$ contains the material parameter c_D, h_D^{sat}, c_L and h_L^{sat}. To understand the behavior of the model, we consider an initial material state with vanishing $\mathscr{H}$ and assume $h_D^{sat} = 0$ and $h_L^{sat} < 0$. If the material is subjected to proportional loading in the direction of $\mathbf{N}_1$ the directional part does not evolve. The first summand in eq.7 is zero since h_D^{sat} is zero and because $\mathscr{H}_D$ is also zero at the beginning of the loading.

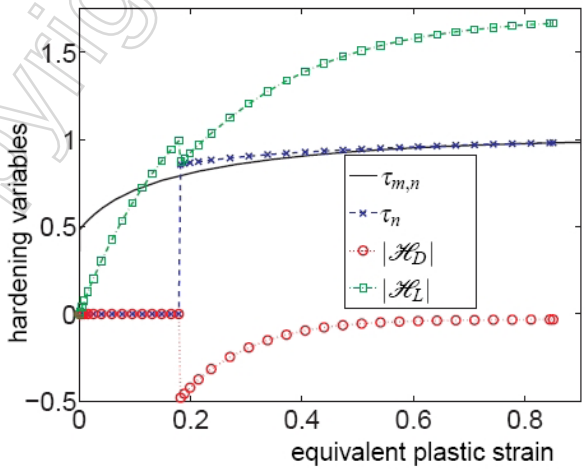

Figure 5: Evolution of the hardening variables for tension followed by shearing

This is confirmed by Fig. 5 which shows the model behavior for a tension-shear simulation. In the tension stage the modulus of $\mathscr{H}_D$ is zero because $\mathscr{H}_D$ does not evolve from the start. $\mathscr{H}_L$ increases right from the beginning of the tension stage. During the orthogonal strain path change from tension to shear the modulus of $\mathscr{H}_D$ suddenly drops to a negative value. This is due to the fact that h_L^{sat} is smaller than zero. For further shearing the modulus of $\mathscr{H}_D$ saturates toward zero. During the orthogonal loading path

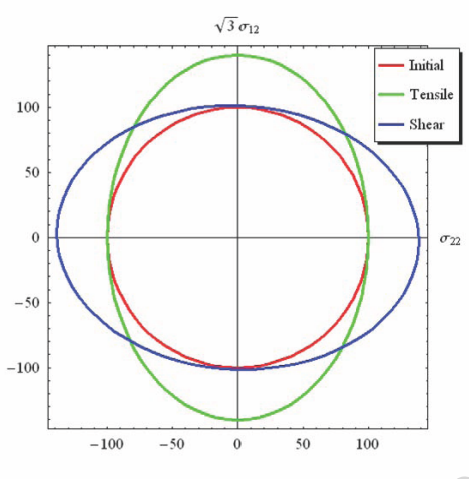

Figure 6: Model behavior in terms of the yield surface evolution

change the modulus of $\mathscr{H}_L$ sustains a small drop before increasing further. The fact that the directional part of $\mathscr{H}$ does not evolve in the first loading stage means that the yield surface does not change in the direction of loading. The principal behavior of the model in this regard is shown in Fig. 6. Let the red curve be the initial yield surface in the $\sigma_{12} - \sigma_{22}$-plane. Loading in the direction of σ_{22} does not change the intersection between the σ_{22}-axis and the yield surface as can be seen easily from the green curve. On the other side an extension of the yield surface in the σ_{12}-direction takes place. This explains how the models takes the cross hardening into account. Even before the orthogonal strain path change from tension to shear takes place the yield surface is extended in the shear direction yielding to an increase in the yield stress and therefore to cross hardening. After the orthogonal strain path change the yield surface shrinks in the direction of re-loading.

2 Model application

2.1 Draw bending

The model was applied to the simulation of a draw bending process where a strip is being pulled from right to left over a roller under tension, where it experiences bending-unbending. Fig. 7 shows the experimental setup.

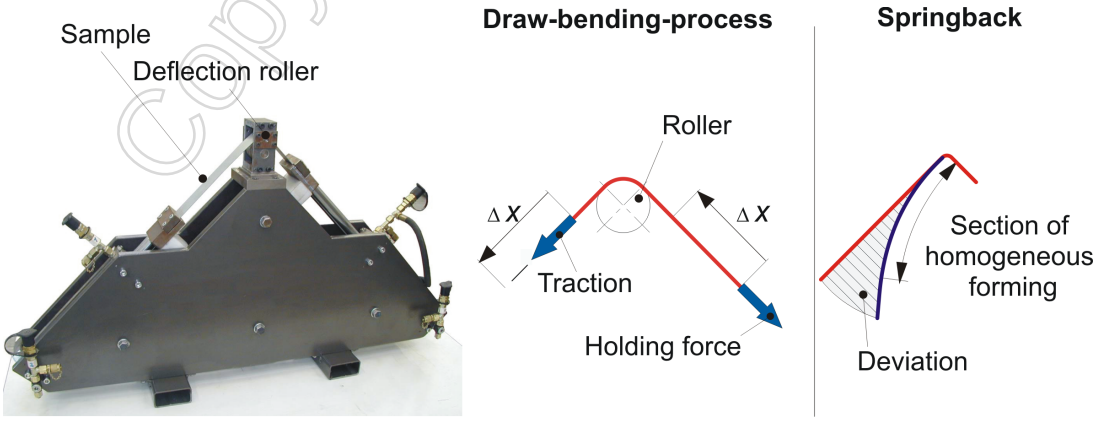

Figure 7: Draw bending device (IUL Dortmund)

The process was simulated in 5 steps by analogy with the experimental procedure. In the first step, the sheet metal strip is pre-bent to 90 degrees using the bending tool. Secondly, the bending tool is

removed. Thirdly, the strip is clamped into the machine at both ends and pulled tight over a rubber roller from both ends, putting it under tension. The actual test begins with the strip being pulled from right to left over the roller under tension, where it experiences bending-unbending. Since the roller moves with the strip, there is little or no friction between them. In the last step, the strip is unclamped and the resulting springback process is simulated. The radius of the roller was 10 mm, the tension on the strip 60 MPa and the drawing distance was 200 mm. The strips were 50 mm broad and had a thickness of 1.6 mm. The simulation was carried out with conventional shell elements. The agreement between the simulations and the draw bending experiments is very good for the distortional and the combined case (Fig. 8). The purely isotropic model results in an overestimate, and the purely kinematic model

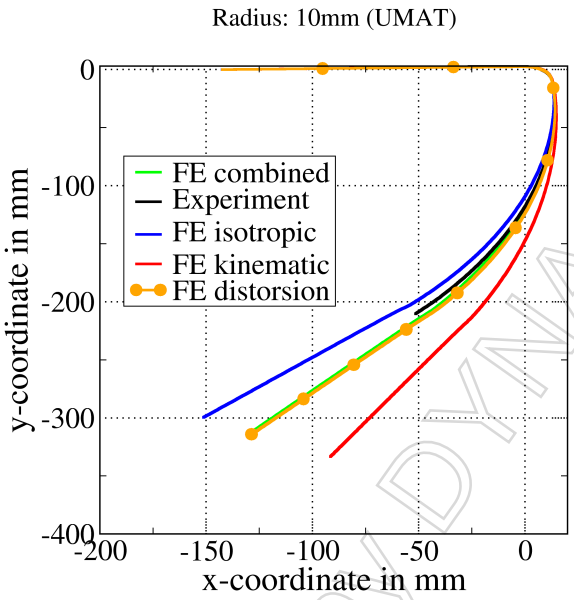

Figure 8: Draw bending (Experiments IUL)

in an underestimate of the amount of springback. In particular, note that the purely isotropic model underestimates the amount of inelastic deformation. In order to satisfy the boundary conditions, then, the amount of elastic deformation is overestimated, resulting in too much springback. Similar results were obtained for other types of steels, e.g., DP 600 [4].

2.2 Deep drawing

The second application is the deep drawing of a cylindrical cup. The details of the geometry for the simulation are according to the experimental setup (Fig. 9).

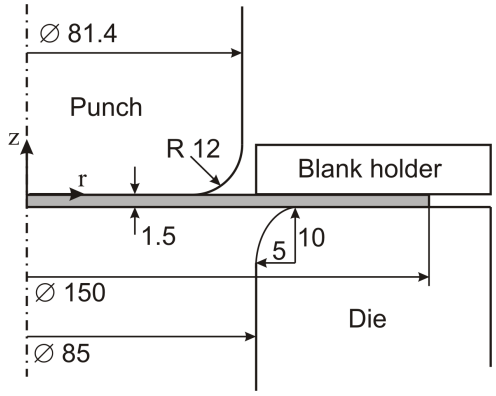

Figure 9: Geometry for the cup-drawing (IUL)

The experimental results were simulated using the finite-element model as described above. Fig. 10 shows the finite-element mesh of the plate. Also indicated in Fig. 10 is the path along which results are displayed. The blank is divided into four quarters which are equally meshed with plane stress shell elements. 17 integration points over the shell thickness have been chosen. The tool, holder and die have all been idealized as rigid bodies here. Contact and friction between the sheet metal workpiece and other parts of the model were modeled using a friction coefficient of 0.05. The blank holder force was 100 kN. Fig. 11 shows the von-Mises stress along the inner surface of the cup for a punch displacement of 45 mm which was the draw depth. All the simulations were carried out with the material model described in this paper but only for the black curve distorsional hardening was activated by the parameter set. The parameter set which underlies the simulation, the result of which is shown by the red curve, is identical to that of the black curve except that c_D, h_D^{sat}, c_L and h_L^{sat} are set to zero. The figure also depicts the result for combined hardening and isotropic hardening. In the case of all hardening mechanisms being activated the von-Mises-stress reaches the highest level especially in regions where the sheet was bend. The red curve and the green curve show qualitatively identical behavior as one would expect since both represent combined hardening. The isotropic hardening probably does not lead to a realistic stress distribution since the draw bending simulation already showed that isotropic hardening alone is not sufficient for a correct modeling of the LH800.

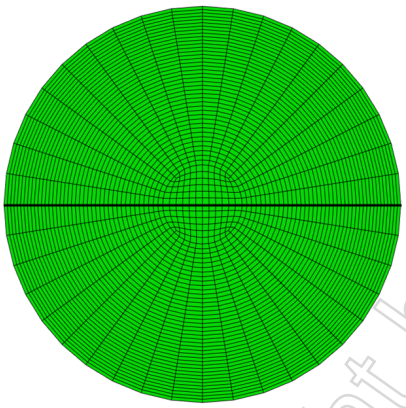

Figure 10: FE-mesh

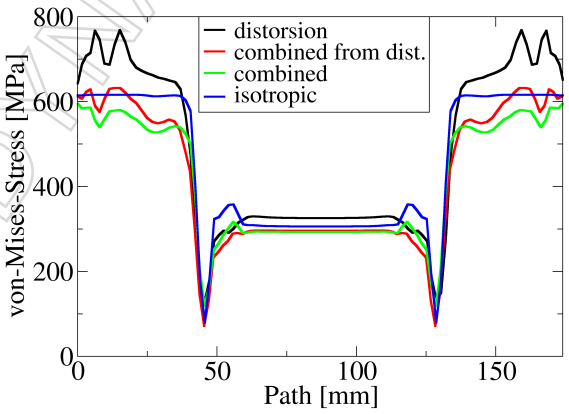

Figure 11: von-Mises stress in deep drawing for different parameter sets

Springback has also been investigated for this process. Due to the geometry there is only little change in shape when the punch is removed. Fig. 12 shows the von-Mises stress at the and of the drawing step and Fig. 13 the same result when the punch is removed. The green and blue color in the flange and bending area (Fig.13) show that the residual stresses are low compared to the stresses at the end of the drawing stage(Fig. 12). The cups in Fig. 12 and Fig. 13 show no earing. This is due to the fact that LH800 shows a very mild initial flow anisotropy which was neglected completely in the simulations.

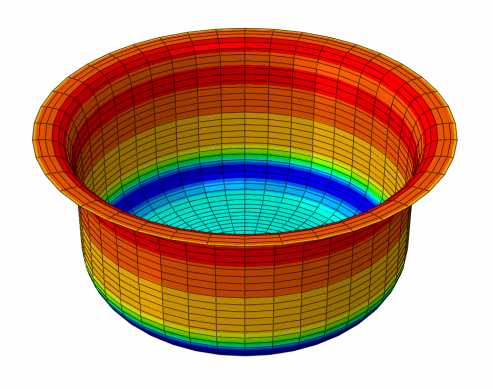

Figure 12: Von-Mises stress before springback

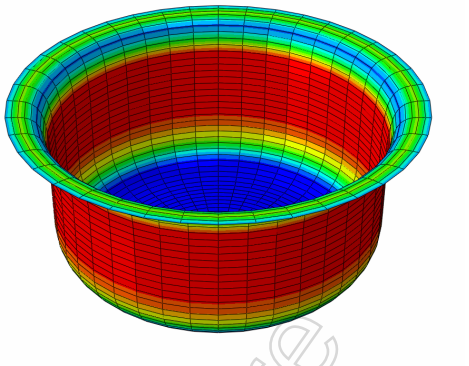

Figure 13: Von-Mises stress after springback

3 Literature

[1] Noman, M.; van Riel, M.; Barthel, C.; Huétink, J.; Svendsen, B.: Experimental characterization and modeling of anisotropic hardening in the ferritic steel LH800, to be sumbmitted, 2009

[2] Cwiekala, T.; Brosius, A.; Tekkaya, A.E.; Grydin, O.; Schaper, M.; Bach, F.-W.; Barthel, C.; Svendsen, B.: Efficient Modelling and Simulation of Process Chains in Sheet Metal Forming and Processing. Steel research int., 79:pp. 731-737, 2008

[3] Levkovitch, V.; Svendsen, B.: Accurate hardening modeling as basis for the realistic simulation of sheet forming processes with complex strain-path changes, Proceedings 9th Numiform Conference, Porto, Portugal, 2007

[4] Wang, J.; Levkovitch, F.; Svendsen, B.: On the modeling and simulation of induced anisotropy in polycrystalline metals with application to springback, Archive of Applied Mechanics 74, pages 890-899, 2005